Cell

Non-Cell-Autonomous Tumor Suppression by p53

Amaia Lujambio,[1,2] Leila Akkari,[2] Janelle Simon,[1,2,4] Danielle Grace,[1,2] Darjus F. Tschaharganeh,[2] Jessica E. Bolden,[1,2] Zhen Zhao,[1,2] Vishal Thapar,[1,2] Johanna A. Joyce,[2] Valery Krizhanovsky,[1,3,*] and Scott W. Lowe[1,2,4,*]
[1]Cold Spring Harbor Laboratory, Cold Spring Harbor, NY 11724, USA
[2]Memorial Sloan-Kettering Cancer Center, New York, NY 10065, USA
[3]Weizmann Institute of Science, Rehovot 76100, Israel
[4]Howard Hughes Medical Institute, New York, NY 10065, USA
*Correspondence: valery.krizhanovsky@weizmann.ac.il (V.K.), lowes@mskcc.org (S.W.L.)
http://dx.doi.org/10.1016/j.cell.2013.03.020

SUMMARY

The p53 tumor suppressor can restrict malignant transformation by triggering cell-autonomous programs of cell-cycle arrest or apoptosis. p53 also promotes cellular senescence, a tumor-suppressive program that involves stable cell-cycle arrest and secretion of factors that modify the tissue microenvironment. In the presence of chronic liver damage, we show that ablation of a p53-dependent senescence program in hepatic stellate cells increases liver fibrosis and cirrhosis associated with reduced survival and enhances the transformation of adjacent epithelial cells into hepatocellular carcinoma. p53-expressing senescent stellate cells release factors that skew macrophage polarization toward a tumor-inhibiting M1-state capable of attacking senescent cells in culture, whereas proliferating p53-deficient stellate cells secrete factors that stimulate polarization of macrophages into a tumor-promoting M2-state and enhance the proliferation of premalignant cells. Hence, p53 can act non-cell autonomously to suppress tumorigenesis by promoting an antitumor microenvironment, in part, through secreted factors that modulate macrophage function.

INTRODUCTION

The p53 tumor suppressor acts as a central node in cellular stress response programs induced by DNA damage and oncogene activation (Vousden and Prives, 2009). p53 binds DNA in a sequence-specific manner and controls the expression of target genes that mediate its diverse effects (Vousden and Prives, 2009). p53 can limit the propagation of premalignant cells by promoting cell-cycle exit or apoptosis, though p53 has other functions that contribute to its tumor-suppressive action depending on context (Li et al., 2012). Consequently, *p53* mutations enable the unrestrained proliferation of damaged cells and thereby promote tumorigenesis in many tissue types.

Cellular senescence is another p53-dependent program that limits tumorigenesis (Collado and Serrano, 2010). Senescence is a form of proliferative arrest that is associated with the stable repression of E2F target genes. However, senescent cells also downregulate the production of extracellular matrix (ECM) proteins, upregulate ECM-degrading enzymes, and secrete a variety of immune modulators and inflammatory cytokines (Coppé et al., 2008), an effect that is mediated by cooperation between p53 and nuclear factor-κB (NF-κB) (Chien et al., 2011; Jing et al., 2011). Collectively, these properties define the senescence-associated secretory phenotype (SASP) and are associated with marked changes in protein secretion (Campisi and d'Adda di Fagagna, 2007).

SASP factors can reinforce the senescence program and influence tissue microenvironment. Thus, key SASP factors can act in an autocrine manner to reinforce senescent growth arrest (Acosta et al., 2008; Kuilman et al., 2008) and/or provoke immune surveillance of the senescent cells, leading to their elimination (Kang et al., 2011; Krizhanovsky et al., 2008; Reimann et al., 2010; Xue et al., 2007). In the context of certain wound-healing responses, SASP limits the extent of tissue damage and facilitates wound resolution (Kong et al., 2012; Krizhanovsky et al., 2008). However, the impact of SASP on malignant initiation or progression is poorly understood, with studies suggesting that the program can be either pro- or antitumorigenic (Coppé et al., 2008; Kang et al., 2011; Krtolica et al., 2001; Xue et al., 2007).

We explore the biology of a stromal-derived SASP program triggered by p53 on cancer initiation in the liver, a well-studied setting in which the microenvironment strongly influences epithelial tumorigenesis (Zhang and Friedman, 2012). In this tissue, tumor initiation is often preceded by hepatic fibrosis resulting from liver damage produced by chronic hepatitis, alcohol, or chemical insults. Here, dying hepatocytes trigger the proliferation of hepatic stellate cells (HSCs), which accumulate in the liver and coordinate the production of ECM components that form the fibrotic scar. During chronic injury, an ongoing cycle of cell death, HSC proliferation, inflammation, and fibrosis eventually leads to organ failure through cirrhosis, which is the strongest risk factor for the emergence of hepatocellular carcinoma (HCC)—the third leading cause of cancer deaths worldwide (Bataller and Brenner, 2005).

We previously implicated a p53-dependent senescence program as part of a tissue homeostatic mechanism that

restricts the extent of fibrosis and facilitates its resolution (Krizhanovsky et al., 2008). Specifically, we observed that, after an initial proliferative phase associated with fibrogenesis, HSCs eventually senesce. We demonstrated that this p53-mediated senescence program limits the extent of fibrosis by halting HSC proliferation through the cell-autonomous action of canonical senescence regulators and the non-cell-autonomous effects of SASP on ECM and immune surveillance. Consistent with this model, mice in which p53 was disabled specifically in HSCs displayed excessive fibrosis following chronic fibrogenic treatment. Here, we evaluate how p53 activity in HSCs influences later stages of liver disease and, ultimately, epithelial cancer development. Our results imply that p53 action can restrict cancer through non-cell-autonomous mechanisms and underscore the interplay between p53 and the tissue microenvironment.

RESULTS

p53 Action in HSCs Limits Fibrosis

To investigate the impact of p53 activity in HSCs during different stages of liver damage, we conditionally deleted p53 expression in murine HSCs. Transgenic mice expressing Cre recombinase from the glial fibrillary acidic protein (*GFAP*) promoter (which, in the liver, is specifically expressed in HSCs) were crossed with mice harboring LoxP sites in introns 1 and 10 of the *p53* gene ($p53^{LoxP/LoxP}$) (Marino et al., 2000). Although the *GFAP* promoter is primarily expressed in the adult astroglia, GFAP-Cre; $p53^{LoxP/LoxP}$ conditional knockout mice show no increased evidence of brain tumors or any other disease (Marino et al., 2000), thus allowing us dissect the role of p53 in HSCs without other confounding phenotypes. Hereafter, GFAP-Cre; $p53^{LoxP/LoxP}$ conditional knockout mice are designated as *HSC-p53*$^{\Delta/\Delta}$, whereas single-transgenic control strains are referred to as GFAP-Cre or p53-LoxP.

We subjected 8-week-old mice to a 6 week treatment with carbon tetrachloride (CCl_4), a well-studied fibrosis-inducing agent (Oakley et al., 2005). Of note, cellular responses to liver damage are highly sex dependent (Naugler et al., 2007), so in most of our analyses, only females were used for comparison. Upon liver damage, HSCs become "activated"—i.e., they differentiate into myofibroblasts, proliferate, and produce the ECM network that constitutes the fibrotic scar (Bataller and Brenner, 2005). As expected, the protocol produced liver fibrosis as assessed by staining with Sirius red, which directly marks the collagen within the ECM, and with hematoxylin and eosin staining (H&E), which is used to evaluate the overall liver morphology (Figure 1A). As quantified by laser scanning cytometry, ~3% of the liver was Sirius-red positive in treated *HSC-p53*$^{\Delta/\Delta}$ mice, representing an ~50% increase over controls (Figure 1B). Similar results were observed when animals were treated with DDC (3,5-diethoxycarbonyl-1,4-dihydrocollidine), a different fibrogenic compound (Figures S1A–S1C available online), though accurate quantification was confounded owing to the appearance of red precipitates in the liver. Livers from *HSC-p53*$^{\Delta/\Delta}$ transgenic mice treated with CCl_4 also showed an expansion of activated HSCs as determined by immunoblotting of α-smooth muscle actin (αSMA) in tissue extracts (Figures 1C and 1D) and increased production of collagen (data not shown). The above findings are consistent with those using the same protocol in which *p53* was ablated in the whole animal or selectively downregulated in HSCs using transgenic RNAi (Krizhanovsky et al., 2008), confirming a role for HSC-expressed p53 in limiting fibrosis.

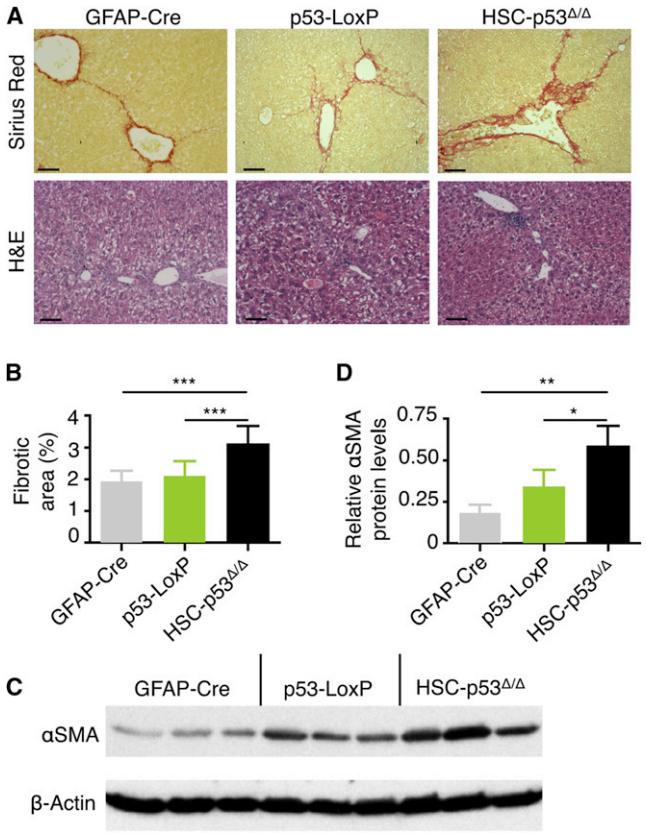

Figure 1. p53 Action in HSCs Limits Fibrosis

(A) Transgenic mice were treated with CCl_4 for 6 weeks, and fibrosis was assessed by Sirius red (top) and H&E (bottom) staining. Scale bars, 100 μm.

(B) Quantification of fibrosis based on Sirius red staining by laser scanning cytometry. At least three liver sections were analyzed per mouse (number of mice: n = 12, GFAP-Cre; n = 14, p53-LoxP; n = 20, *HSC-p53*$^{\Delta/\Delta}$). Values are mean + SD.

(C and D) Immunoblot showing expression of αSMA in the livers of mice treated with CCl_4 for 6 weeks (C). Quantification of αSMA relative to β-actin levels using ImageJ software (D). Values are mean + SD.

H&E, hematoxylin and eosin; αSMA, α-smooth muscle actin.

See also Figure S1.

p53 Activity in HSCs Restrains Cirrhosis

The excessive ECM produced by HSCs during chronic liver damage disrupts liver architecture, preceding frank cirrhosis and eventual liver failure. Cirrhosis is associated with a grossly disrupted liver architecture and parenchymal destruction and can be accompanied by the aberrant retention of fluids in the abdominal cavity (ascites), as well as pathognomonic serum levels of proteins and enzymes produced by the liver (Bataller and

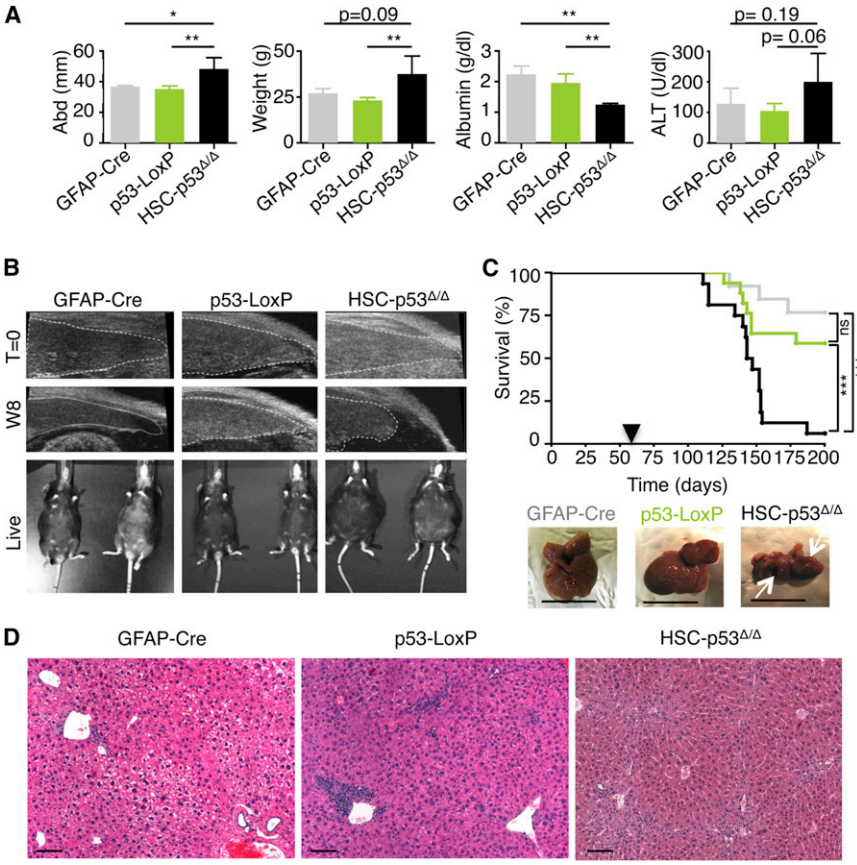

Figure 2. p53 Activity in HSCs Restrains Cirrhosis

(A) Abdomen width and mouse weight (week 8) and ALT and albumin levels (week 13) in mice treated with CCl_4. Values are mean + SD, n = 4, GFAP-Cre; n = 5, p53-LoxP; n = 3, *HSC-p53*$^{\Delta/\Delta}$.

(B) Ultrasound imaging of transgenic mice treated with CCl_4 (week 8 of treatment). The live whole-mouse images show ascites only in representative *HSC-p53*$^{\Delta/\Delta}$ male mice.

(C) Kaplan-Meier curve documenting survival of mice treated with CCl_4. Arrowhead indicates beginning of CCl_4 treatment. Statistical comparison of Kaplan-Meier curves is based on the log rank test. Representative livers are displayed (white arrows represent liver retraction). Scale bars, 1 cm. GFAP-Cre in gray, n = 14; p53-LoxP in green, n = 20; *HSC-p53*$^{\Delta/\Delta}$ in black, n = 19.

(D) *HSC-p53*$^{\Delta/\Delta}$, but not single-transgenic (GFAP-Cre and p53-LoxP), mice treated with CCl_4 exhibited disrupted liver histology evaluated by H&E staining. Scale bars, 100 μm.

W8, week 8; abd, abdomen width; n, number of mice; ALT, alanine transaminase; H&E, hematoxylin and eosin.

See also Figure S2.

Brenner, 2005). To study HSC-specific functions of p53 in more advanced stages of liver damage, we challenged male and female mice by treating them twice a week with CCl_4, a chronic regimen known to produce cirrhosis after 12 weeks of treatment (Oakley et al., 2005). By 13 weeks, most of CCl_4-treated *HSC-p53*$^{\Delta/\Delta}$ females displayed signs of overt ascites (Figure 2A), as well as abdominal distension and weight gain when compared to similarly treated controls (Figure 2A). Accordingly, liver damage in *HSC-p53*$^{\Delta/\Delta}$ mice was more pronounced, as indicated by decreased serum albumin and increased alanine transaminase levels measured after 13 weeks of treatment (Figure 2A). These pathological changes were obvious much earlier in male mice, which are more susceptible to liver damage (Naugler et al., 2007). In fact, in *HSC-p53*$^{\Delta/\Delta}$ males, retraction of the liver was identified by ultrasound examination as early as week 8 of treatment (Figure 2B).

The excessive liver damage occurring in *HSC-p53*$^{\Delta/\Delta}$ mice was associated with increased mortality. Although a few single-transgenic females exposed to CCl_4 died within 90 days (Figure 2C), the vast majority survived beyond 200 days. By contrast, most *HSC-p53*$^{\Delta/\Delta}$ mice died within the first 90 days of CCl_4 exposure (Figure 2C). Histological examination of *HSC-p53*$^{\Delta/\Delta}$ livers revealed a disrupted cytoarchitecture when compared to single-transgenic controls (Figure 2D). *HSC-p53*$^{\Delta/\Delta}$ mice showed more extensive fibrosis, pointing to liver failure as the likely cause of death. Together, these results indicate that p53 activity in HSCs acts to protect organ function following liver damage.

Further characterization of liver pathology in moribund *HSC-p53*$^{\Delta/\Delta}$ mice revealed the presence of small tumors rarely seen in controls (Figures S2A and S2B; p = 0.029 and p = 0.017, relative to GFAP-Cre and p53-LoxP, respectively). Histological analyses could not determine the precise origin of these tumors, and their enrichment on the liver surface suggested that they might have infiltrated from an extrahepatic site (Figure S2A). To determine whether these tumors may have been triggered by aberrant Cre-activation and *p53* recombination, we performed PCR analysis of tumor DNA to assess the status of the conditional *p53* allele. Interestingly, 60% of the tumors retained intact *p53* genes (Figures S2C and S2D). Thus, *p53* deletion in HSCs appeared to create a liver environment that promotes tumorigenesis.

p53 Activity in HSCs Limits Epithelial Tumorigenesis

The above results prompted us to study how HSC-expressed p53 influences liver tumor development. To specifically produce tumors in the epithelial compartment, we modified our approach by combining CCl_4 fibrogenic treatment with coadministration of the carcinogen diethylnitrosamine (DEN) (Figure 3A). This carcinogen generates tumors in mice resembling aggressive HCC as assessed histopathologically and by gene expression profiling (Lee et al., 2004). To rule out the possibility that aberrant Cre activation (and hence *p53* gene deletion) contributes to tumor formation in these cells, we used the compound transgenic *HSC-p53*$^{\Delta/\Delta}$;Rosa26-LSL-LacZ, which allowed us to trace cells in which GFAP-Cre allele was active by conventional β-galactosidase (β-gal) staining. The resulting mice were treated with the

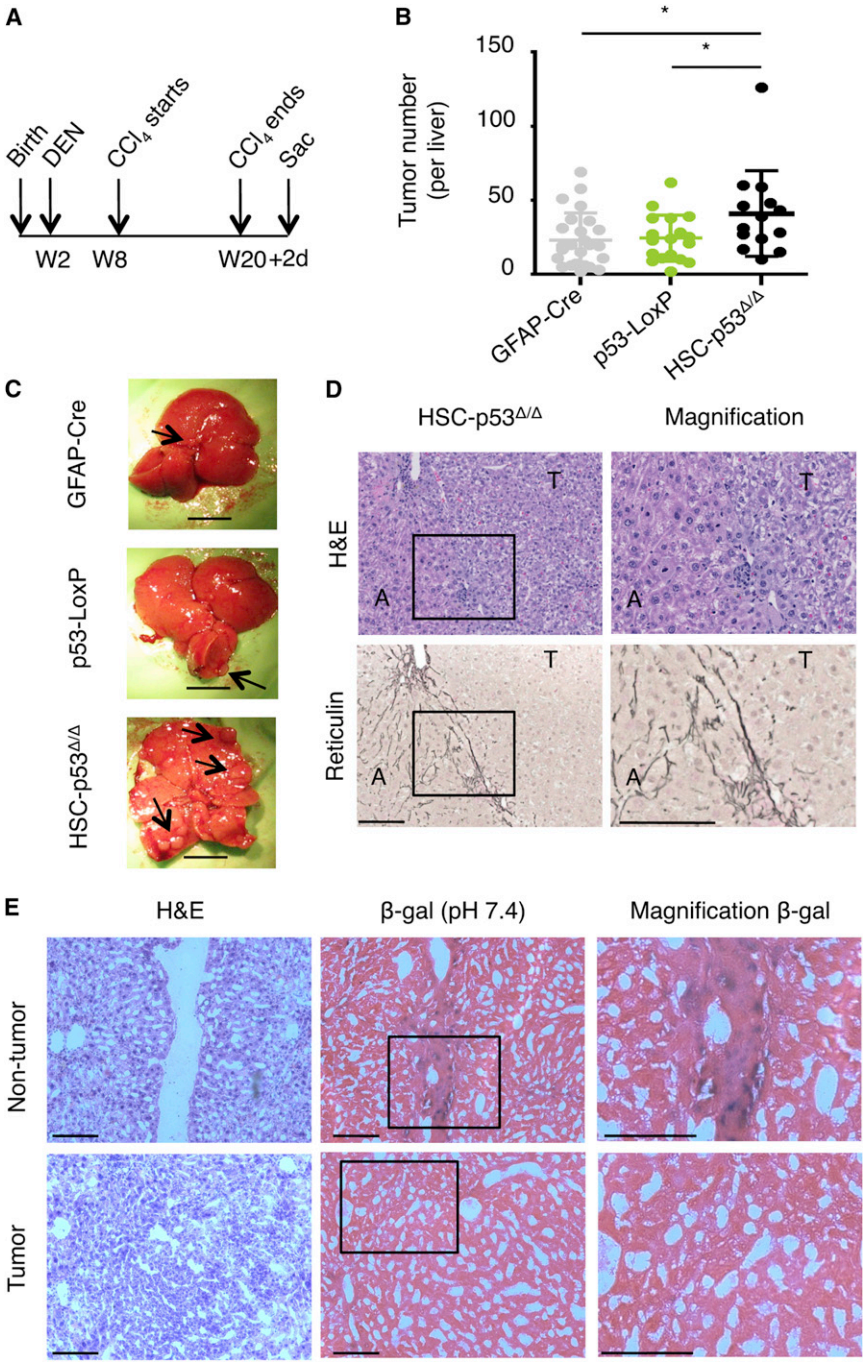

Figure 3. p53 Activity in HSCs Limits Epithelial Tumorigenesis

(A) Schematic diagram indicating the time points for DEN and CCl_4 treatment.

(B and C) Number of macroscopic tumors. Scatterplot representation: dots indicate individual animals and bars mean ± SD. If the top and bottom values are deleted in all groups: p = 0.0119 (GFAP-Cre versus *HSC-p53*$^{\Delta/\Delta}$) and p = 0.0039 (p53-LoxP versus *HSC-p53*$^{\Delta/\Delta}$). If the outlier in *HSC-p53*$^{\Delta/\Delta}$ mice is removed: p = 0.0640 (GFAP-Cre versus *HSC-p53*$^{\Delta/\Delta}$) and p = 0.0318 (p53-LoxP versus *HSC-p53*$^{\Delta/\Delta}$). Representative livers from the three genotypes are displayed. Scale bars, 1 cm. Black arrows indicate tumors.

(D) H&E (top) and reticulin (bottom) staining of a representative liver from treated *HSC-p53*$^{\Delta/\Delta}$ mice. Right, magnification of the boxed area on the left. Scale bars, 100 μm.

(E) Liver tissues (H&E staining, left) were stained for transgenic Lac-Z expression (β-gal staining). β-gal positive HSCs accumulated in the fibrotic scars (top). However, liver tumor cells were β-gal negative, indicating absence of recombination events. *HSC-p53*$^{\Delta/\Delta}$;R26-LSL-Lacz triple-transgenic mice were used, and 36 livers were analyzed.

W, weeks; D, days; H&E, hematoxylin and eosin; T, tumor; A, adjacent liver; β-gal, β-galactosidase. See also Figure S3.

regimen shown in Figure 3A, with DEN being administered 15 days after birth and CCl_4 provided for 12 weeks, starting 42 days later. Animals were sacrificed 2 days after the last CCl_4 injection (day 142), and their livers were examined for tumor incidence and histology.

Despite the initiation of the fibrogenic treatment several weeks after administration of the carcinogen, *HSC-p53*$^{\Delta/\Delta}$ livers showed nearly 2-fold more tumors when compared to controls (Figures 3B and 3C; p = 0.022 and p = 0.015, relative to GFAP-Cre and p53-LoxP). All of the analyzed tumors were of epithelial origin with an HCC histology, showing typical reticulin loss within the tumor nodules (n = 147; Figures 3D and S3A). These tumors were not β-gal positive (n = 36 tumors analyzed from seven *HSC-p53*$^{\Delta/\Delta}$;Rosa26-LSL-LacZ mice; Figure 3E) and showed no evidence of *p53* gene deletion (Figure S3B). By contrast, β-gal expression was observed in fibrotic regions of the treated livers consistent with efficient Cre-mediated recombination in the HSC compartment. Although the incidence of tumors was increased in *HSC-p53*$^{\Delta/\Delta}$ mice, overall size and grade were similar to the control genotypes (data not shown). These observations imply that p53 action in HSCs can reduce HCC initiation, thereby restricting tumorigenesis in a non-cell-autonomous manner.

p53 Regulates SASP of HSCs and Genes Affecting Macrophage Function

The ability of p53 to act non-cell autonomously to suppress tumorigenesis suggests that it engages a program that influences tissue microenvironment, perhaps via its action on senescence and SASP. As a first step toward understanding

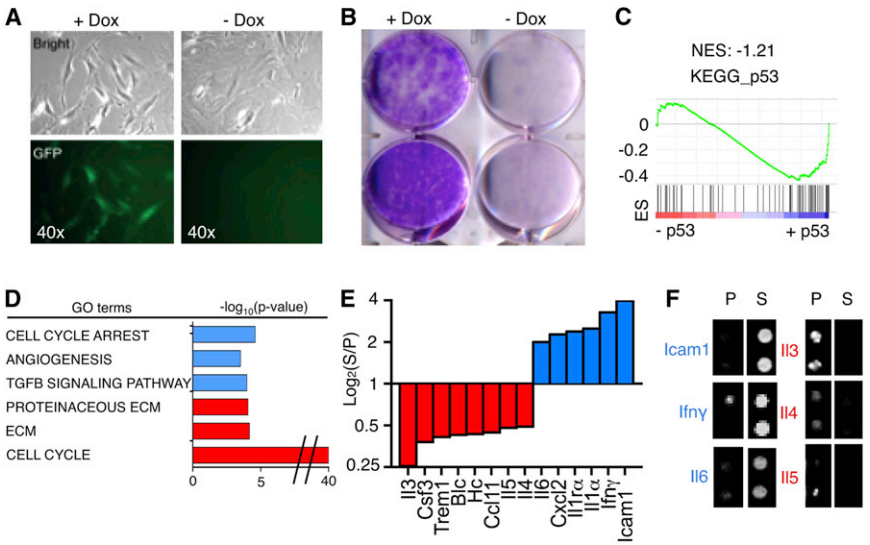

Figure 4. p53 Regulates SASP of HSCs and Genes Affecting Macrophage Function

(A) Activated HSCs from CMV-rtTA;TG-p53.1224 mouse in the presence or absence of Dox (proliferating or senescent, respectively) by phase-contrast microscopy for changes in morphology (top) and expression of GFP (bottom).

(B) Activation of p53 was sufficient to restrict colony formation as assessed by crystal violet staining 10 days after plating.

(C) GSEA plot evaluating changes in p53 pathway (KEGG_p53) depending on p53 expression.

(D) GO analysis of genes significantly downregulated (red) or upregulated (blue) upon p53 expression. Differentially expressed genes were identified by comparing senescent (blue) versus proliferating (red) HSCs. Representative examples are displayed.

(E and F) Murine cytokine array for conditioned media from proliferating versus senescent HSCs. Bars represent the average of intensity of two independent experiments (log_2). Factors showing 2-fold increase (blue) or decrease (red) on senescent versus proliferating HSCs are shown. In the right, representative blots from the cytokine array (F).

ES, enrichment score; NES, normalized enrichment score; S, senescent; P, proliferating.

See also Figure S4 and Table S1.

mechanism, we determined how p53 action influences gene expression in HSCs. We crossed transgenic mice harboring a tetracycline-response-element (TRE)-driven short-hairpin RNA (shRNA) that efficiently represses p53 expression (TG-p53.1224) to mice expressing rtTA (a reverse tetracycline-controlled transactivator transgene) from the cytomegalovirus promoter (Figure S4A) (Premsrirut et al., 2011). HSCs were purified from an adult mouse by gradient centrifugation and subjected to cell culture in the presence of doxycycline (Dox), conditions in which p53 expression was suppressed (Figure S4B). This system enables p53 activity to be controlled in HSCs simply by the addition and removal of Dox.

In the presence of Dox, activated HSCs were GFP positive and were highly clonogenic. Upon Dox withdrawal, GFP expression was rapidly reduced, and HSCs accumulated high levels of p16, p21, and SA-β-gal (senescence-associated β-gal) activity and eventually stopped proliferating with the characteristic morphology of senescent cells (Figures 4A, 4B, and S4C). Transcriptional profiling of proliferating versus senescent HSC preparations (n = 3 per each condition) confirmed that both sets of HSCs expressed high levels of the HSC markers αSMA (Figure S4C), vimentin, and vinculin (data not shown). Gene set enrichment analysis (GSEA) revealed significant similarities between p53-arrested HSCs and the "KEGG_p53" pathway gene set, as well as a previously identified senescence signature (Figures S4C and S4D and Tables S1A and S1B) (Fridman and Tainsky, 2008). Thus, Dox removal efficiently activated p53, leading to senescence.

The transcriptional profiles were subject to gene ontology (GO) analysis to systematically identify potential processes affected by p53. Genes downregulated by p53 showed a significant enrichment for the GO term "cell cycle" (Figure 4D and Table S1C) and included many E2F targets. Indeed, GSEA using a list of established E2F target genes confirmed that these are significantly underexpressed in senescent HSCs (Table S1D). Alternatively, genes upregulated by p53 showed enrichment for the GO terms "extracellular matrix," "proteinaceous extracellular matrix," and "extracellular matrix structural constituent" (Figure 4D and Table S1C). The ability of p53 to repress cell cycle and ECM genes in senescent murine HSCs is consistent with gene expression profiles from human HSCs (Krizhanovsky et al., 2008) and its ability to limit a fibrogenic response.

Genes upregulated in p53-expressing HSCs included biological processes such as cell-cycle arrest, which have previously been linked to p53 action and/or senescence (Figure 4D and Table S1E). Interestingly, "Activation_of_immune_response" and "Activation_of_NF-κB_transcription_factor" gene sets were enriched in senescent HSCs (Figure S4E and Table S1F). This same analysis identified genes associated with "exocytosis" and "Vesicle_mediated_transport" as overrepresented in senescent HSCs (Figure S4E and Table S1F). All of these observations suggest that p53 can directly or indirectly affect protein secretion and modulate immune signaling (Krizhanovsky et al., 2008).

To measure protein secretion, we subjected conditioned media (CM) from p53-suppressed or p53-activated HSCs to a murine antibody array that detects secreted cytokines and chemokines (Figures 4E, 4F, and S4F). Senescent HSCs preferentially secreted Il6, Icam1, and Ifnγ, whereas proliferating HSCs secreted Il3, Il4, and Il5, among other factors, in agreement with previously reported secretion profiles (Chien et al., 2011; Coppé et al., 2008; Crescenzi et al., 2011). The most notable changes involved factors known to influence the differentiation and activity of macrophages (e.g., Il6, Ifnγ, and Il4 [Qian and Pollard, 2010]), a cell type known to modulate liver fibrosis (Duffield

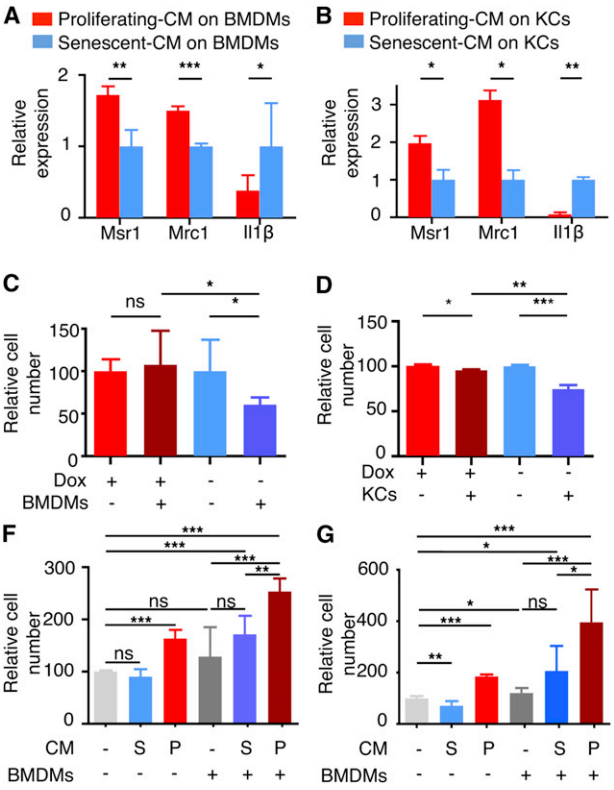

Figure 5. p53 Signaling through SASP Modulates Macrophage Polarization and Function

(A and B) Quantitative RT-PCR of *Msr1*, *Mrc1*, and *Il1β* expression in BMDMs (A) or KCs (B) exposed to CM from proliferating (red) or senescent (blue) HSCs. Data are relative to expression of BMDMs with CM from senescent HSCs, normalized to the average expression of the housekeeping genes *Hprt* and *Ubc*. Values are mean + SD from three independent experiments.

(C and D) BMDMs (C) and KCs (D) exhibited preferential cytotoxic activity against senescent HSCs (blue) when compared to proliferating HSCs (red). Viable cell numbers are shown and are relative to the number of viable cells without macrophages. Values are mean + SD from two independent experiments performed in triplicate.

(E) Sequence of movie frames displaying the targeting of a senescent HSC (green cell; white arrow) by BMDMs (red cells; red arrows).

(F and G) Cell viability in a coculture experiment: premalignant cells were incubated with CM from proliferating (red) or senescent (blue) HSCs and were cocultured with (+) or without (–) BMDMs. Two independent experiments were performed in triplicate for two different cell lines (F and G). Viable cell numbers are shown and are relative to the number of viable cells cultured without BMDMs and with normal media; values are mean + SD.

BMDM, bone-marrow-derived macrophages; KCs, Kupffer cells; CM, conditioned media; Ren, renilla; S, senescent; P, proliferating.

See also Figure S5 and Movies S1, S2, S3, and S4.

et al., 2005). Of note, the preferential secretion of IL6 and IFNγ was confirmed in senescent human HSCs (Figures S4G and S4H), highlighting the relevance of these findings to the human setting.

p53 Signaling through SASP Influences Macrophage Polarization

The data described above suggest that the SASP program triggered by p53 might influence macrophage function and/or polarization. Macrophages are myeloid cells that function in innate immunity by phagocytizing cellular debris and pathogens and stimulating the adaptive immune response (Biswas and Mantovani, 2010; Qian and Pollard, 2010). In cancer, these subclasses can have different effects on tumorigenesis and antitumor immunity. In general, "classically activated" M1 macrophages have natural roles in pathogen defense and display antitumor activity, whereas "alternatively activated" M2 macrophages can promote angiogenesis and tissue remodeling, thereby supporting tumor progression and metastasis. Ifnγ favors M1 polarization, whereas Il4 and Il13 trigger M2 polarization. These macrophage subclasses can be distinguished by the differential expression of gene markers: M1 macrophages express higher levels of inflammatory and antiangiogenic cytokines such as *Il1β*, whereas M2 macrophages express arginase-1 (*Arg1*), mannose receptor-1 (*Mrc1*), and macrophage scavenger receptor 1 (*Msr1*) (Movahedi et al., 2010).

We next determined how factors secreted from proliferating or senescent HSCs affected macrophage polarization. As damaged livers are composed of resident (Kupffer cells, KCs) and infiltrating macrophages (bone-marrow-derived macrophages, BMDMs), we studied the effects of HSCs on both macrophage populations. Two genes associated with M2 phenotype, *Mrc1* and *Msr1*, were upregulated in macrophages incubated with CM from proliferating HSCs compared to macrophages exposed to CM from senescent HSCs (Figures 5A, 5B, S5A, and S5B). Conversely, when macrophages were exposed to CM from senescent HSCs, a significant increase in the M1-marker *Il1β* was observed (Figures 5A and 5B). Thus, p53 activation in HSCs shifts their secretory profile from supporting M2 to M1 polarization. Such changes might be important at different stages of the fibrogenic response but have the net effect of promoting the tumor-inhibitory macrophage subtypes when *p53* is intact.

p53-Activated M1-like Macrophages Eliminate Senescent Cells

To evaluate the effects of p53 on "HSC-macrophage" interactions, we cocultured either resident (KC) or infiltrating (BMDM) macrophages with proliferating or senescent HSCs for 24–48 hr and examined their proliferation and survival by cell quantification and time-lapse video microscopy. Although the presence of macrophages (BMDMs and KCs) had little effect on the accumulation of proliferating HSCs, they showed a marked

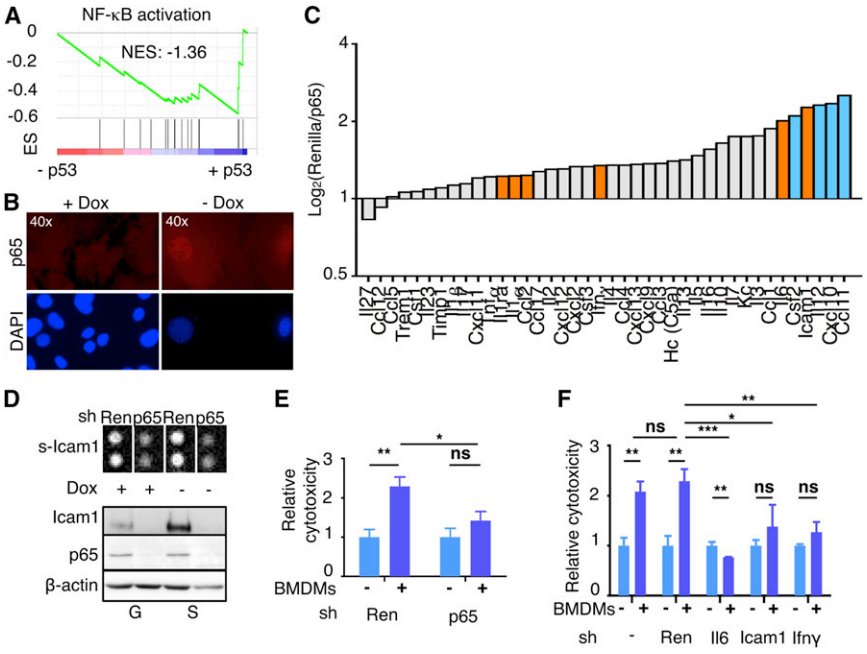

Figure 6. NF-κB Mediates p53-Dependent SASP

(A) GSEA plots evaluating p53-dependent changes in NF-κB signaling pathway.

(B) Immunostaining of proliferating (+Dox) and senescent HSCs (−Dox) with anti-p65 antibody (top) and counterstained with DAPI (bottom) to show nuclear NF-κB accumulation and SAHF formation, respectively, in senescent HSCs.

(C) Murine cytokine array for conditioned media from senescent HSCs transduced with *Renilla* or *p65* shRNA. Bars represent the average of two independent experiments (log_2). Factors upregulated in senescent HSCs (Figure 4E) are indicated in orange.

(D) Top, cytokine array blot extract showing secreted Icam1 in cells transduced with *Renilla* or *p65* shRNA, in proliferating or senescent HSCs. Bottom, p65 and Icam1 protein levels in the same cells. β-actin serves as loading control.

(E and F) Cytotoxicity of senescent HSCs (blue) infected with shRNAs (*Renilla* and *p65* in E; *Renilla*, *Il6*, *Ifnγ*, and *Icam1* in F) and incubated with (+) or without (−) BMDMs. The cytotoxicity (dark blue) is relative to the basal cytotoxicity (light blue, in the absence of incubation with BMDMs, which has been normalized to 1). Values are mean + SD from triplicates.

ES; enrichment score; NES, normalized enrichment score; Ren, renilla; BMDM, bone-marrow-derived macrophages.

See also Figures S4 and S6 and Table S1.

ability to eliminate senescent HSCs (Figures 5C–5E and Movies S1, S2, S3, and S4). Similarly, BMDM were more effective at targeting primary $p53^{+/+}$ HSCs, which senesce in culture, than their $p53^{-/-}$ counterparts, confirming that p53-mediated senescence stimulates HSC elimination by macrophages (Figures S5C–S5E). Additionally, natural killer (NK) cells preferentially target senescent human (Chien et al., 2011; Krizhanovsky et al., 2008) and murine HSCs (Figure S5F), implying that p53 action in senescent cells triggers altered surveillance by multiple immune cell types.

If p53 action in HSCs contributes to an antitumor microenvironment through its impact on macrophage polarization, we hypothesized that "HSC-macrophage" interactions might alter the proliferation or survival of premalignant cells. To test this, we exploited two premalignant hepatoblast progenitor lines previously used in our laboratory to identify new tumor suppressor genes in HCC (Zender et al., 2008). These cells were cocultured with BMDMs, incubated with CM from either growing or senescent HSCs, and quantified 48 hr later. The combination of BMDMs with CM from proliferating HSCs enhanced proliferation of premalignant cells when compared to BMDMs with CM from senescent HSCs or BMDMs with control media (Figures 5F and 5G). This outcome could not be explained by the individual or the additive effects of CM from proliferating HSCs or BMDMs alone on premalignant cell proliferation but rather is explained by the significant interaction between both parameters (interaction p value: p = 0.0470 [Figure 5F] and p = 0.0027 [Figure 5G]). Hence, in this assay, p53 action and senescence in HSCs reduces their ability to stimulate a proproliferative microenvironment.

p53 and NF-κB Cooperate to Induce SASP and Influence Macrophage Function

To further understand how p53 influences the tissue microenvironment, we studied the regulation of SASP genes in HSCs. Whereas some of these genes are direct p53 targets (e.g., *Icam1*), others have not been directly linked to p53. We and others have identified a crucial role for NF-κB in the control of SASP and have shown that p53 cooperates with NF-κB to trigger senescence (Acosta et al., 2008; Chien et al., 2011; Jing et al., 2011). Accordingly, several factors selectively secreted by senescent cells—Il6, Icam1, and Ifnγ—are known NF-κB targets (Chien et al., 2011; Crescenzi et al., 2011), and GSEA confirmed that NF-κB signaling was highly upregulated in senescent HSCs (Figure 6A). As has been observed in other contexts (Ryan et al., 2000), p53 triggered NF-κB activation as assessed by the nuclear accumulation of the NF-κB subunit p65 (Figures 6B and S6A). How this occurs in HSCs remains to be determined, though we note that several genes upregulated in senescent HSCs (e.g., *Eda2r* or *Pycard*) are known NF-κB activators and either established p53 targets (Ohtsuka et al., 2004; Tanikawa et al., 2009) or (e.g., *Tnf*, *Camk2a*, *Card11*, and *Ikbkb*) harbored consensus p53-binding motifs (Figures S6B and S6C and Table S1G).

To further explore the role of NF-κB in controlling SASP, we determined how suppression of the essential NF-κB component $p65^{RelA}$ affected expression of SASP factors and the targeting of senescent HSCs by BMDMs. shRNAs targeting p65 were cloned into the retroviral vector LMN (Figure S6D), and a *Renilla luciferase* shRNA was used as a neutral control. Upon p53 activation, cells expressing p65 shRNAs showed reduced

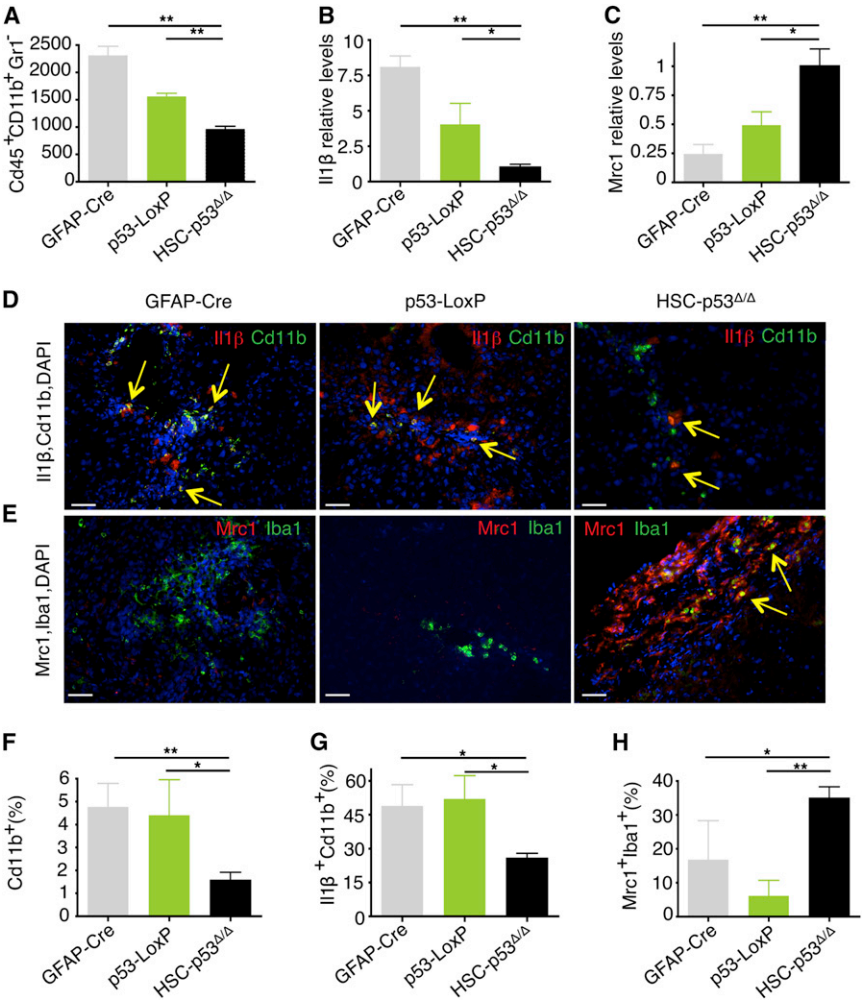

Figure 7. p53 Activity in HSCs Promotes an Antitumor Microenvironment

(A) Quantification of viable $Cd45^+Cd11b^+Gr1^-$ cells in CCl_4-treated mice (n = 3 from each genotype). Values are mean + SD.

(B and C) Quantitative RT-PCR of FACS-sorted $Cd45^+Cd11b^+Gr1^-$ cells for *Il1β* (B) and *Mrc1* (C) expression. The results are normalized to the average expression of the housekeeping genes *Hprt* and *Ubc* and are relative to the expression in *HSC-p53*$^{\Delta/\Delta}$ mice. Values are mean + SD of three independent livers per genotype.

(D–H) Staining for Cd11b (red) and Il1β (green) (D) and Iba1 (red) and Mrc1 (green) (E), revealing less $Cd11b^+$ or $Iba1^+$ macrophages, less $Cd11b^+Il1\beta^+$ macrophages, and more $Iba1^+Mrc1^+$ macrophages in *HSC-p53*$^{\Delta/\Delta}$ CCl_4-treated livers than in control livers. Quantification of $Cd11b^+$ cells (% of total $DAPI^+$ cells) (F), $Cd11b^+Il1\beta^+$ cells (% of total $Cd11b^+$ cells) (G), and $Mrc1^+Iba1^+$ cells (% of total Iba^+ cells) (H). Scale bars, 100 μm. Yellow arrows indicate double-stained cells. Values are mean + SD.

See also Figure S7.

expression and secretion of Icam1 and Il6 (Figures 6C, 6D, and S6E) compared to cells expressing the control shRNA. p65 suppression also reduced the abundance of Ifnγ mRNA, though the effect of this treatment on Ifnγ secretion was modest (Figures 6C, 6D, and S6E). Accordingly, p65 knockdown had no effect on the viability of proliferating HSCs that were cocultured with BMDMs (data not shown) but rescued the cytotoxic effect of BMDMs on senescent HSCs (Figure 6E). Similar results were obtained when using shRNAs against the NF-κB targets *Il6*, *Icam1*, or *Ifnγ* (Figures 6F and S6F), indicating that the ability of macrophages to target senescent HSCs is a direct SASP effect and not merely a consequence of cell-cycle arrest. These results support the antitumorigenic role of NF-κB in senescent cells (Chien et al., 2011; Jing et al., 2011) and highlight the cooperation between NF-κB and p53 in executing the senescence program.

p53 Activity in HSCs Promotes an Antitumor Microenvironment

The ability of p53 to influence macrophage polarization raised the possibility that *p53* status in HSCs might influence the composition of macrophage subpopulations in damaged livers. To examine this, we used fluorescence-activated cell sorting (FACS) to quantify, isolate, and characterize $CD45^+Cd11b^+Gr1^-$ macrophages from CCl_4-treated livers. Surprisingly, total macrophage populations were significantly decreased in *HSC-p53*$^{\Delta/\Delta}$ livers when compared to GFAP-Cre and p53-loxP controls (Figures 7A and S7A; p = 0.002 and p = 0.002, respectively). Using a quantitative RT-PCR assay of macrophage polarization markers to assess the relative abundance of macrophage subtypes in these sorted populations, we observed that those macrophages present in the control GFAP-Cre and p53-loxP livers showed higher expression levels of the M1-marker *Il1β* (Figure 7B; p = 0.001 and p = 0.043, respectively), whereas *HSC-p53*$^{\Delta/\Delta}$ livers were enriched for the M2-marker *Mrc1* (Figure 7C; p = 0.012 and p = 0.048, respectively).

These results were confirmed by directly analyzing liver sections using immunofluorescence with antibodies recognizing different macrophage subpopulations (Figures 7D, 7E, S7B, and S7C). The percentage of cells expressing the general macrophage markers Cd11b or Iba1 was reduced in *HSC-p53*$^{\Delta/\Delta}$ livers (Figure 7F; p = 0.004 and p = 0.027 relative to GFAP-Cre and p53-LoxP, respectively). More than 50% of $Cd11b^+$ macrophages in the GFAP-Cre and p53-LoxP mice were also positive for the M1-marker *Il1β*, whereas only 25% of macrophages present in *HSC-p53*$^{\Delta/\Delta}$ livers were *Il1β* positive (Figures 7D, 7G, and S7B; p = 0.017 and p = 0.014, respectively). By contrast, more than 35% of the macrophages present in *HSC-p53*$^{\Delta/\Delta}$ livers expressed the M2-marker Mrc1, compared to only 5%–15% of these cells in GFAP-Cre and p53-LoxP livers (Figures 7E, 7H, and S7C; p = 0.0423 and p = 0.0012 when compared to GFAP-Cre and p53-LoxP, respectively). Still, not all macrophage

populations could be identified using these markers, suggesting that yet other macrophage subclasses might be present in damaged livers (Ramachandran et al., 2012). Regardless, p53 action in HSCs can trigger a quantitative and qualitative enrichment of antitumor M1 macrophages in damaged livers, which could, in part, explain the non-cell-autonomous tumor-suppressive effects of p53.

DISCUSSION

The mechanisms that link chronic inflammatory responses to tumorigenesis remain a subject of intense investigation, underscoring the need to better understand complex functional interactions that occur between different cell types in tissues. Following chemical injury to the liver, quiescent HSCs, which are of mesenchymal origin, enter the cell cycle, differentiate, and sustain a chronic inflammatory response accompanied by fibrosis (Zhang and Friedman, 2012). In the face of continued stress, a cycle of persistent injury, hepatocyte death, and further HSC expansion can induce cirrhosis and generate a microenvironmental milieu that provides fertile ground for HCC formation. Although proliferating HSCs initially contribute to the inflammatory response, their eventual p53-dependent senescence restrains fibrosis, organ failure, and hepatic tumorigenesis.

Aberrant activation of *Cre* in hepatocytes cannot explain the increased propensity of *HSC-p53*$^{\Delta/\Delta}$ mice to epithelial tumor development because the HCCs arising in Cre-expressing mice showed no evidence of recombination at the *p53* locus. Although Cre-activatable lacZ reporter expression was detected in fibrotic areas of livers derived from tumor-bearing mice, none of the epithelial tumors were LacZ positive. Hence, p53 can act to suppress tissue damage and ultimately tumorigenesis in a non-cell-autonomous manner. These results are consistent with the observation that MCF7 breast cancer cells produce more tumors when injected subcutaneously into p53 null mice compared to wild-type controls (Kiaris et al., 2005) and are reminiscent of studies supporting a non-cell-autonomous role for Pten in suppressing breast cancer development in transgenic mice (Trimboli et al., 2009).

Nonetheless, the *Cre* transgene alone may impact tumorigenesis in different ways. Hence, in some experiments, we noted differences in the behavior of our GFAP-Cre and p53-LoxP control strains (e.g., see Figures 1C, 1D, and 7A–7C). This effect was most notable in male mice, which are substantially more tumor prone than females (Naugler et al., 2007), and GFAP-Cre mice showed a significant decrease in tumors compared to p53-loxP animals, confounding comparisons between tumors in this gender (data not shown). Though the basis for the male bias remains unclear, we suspect that some form of Cre-mediated damage impacts the proliferation of HSCs as has been seen in some other settings (Forni et al., 2006). Mice harboring *Cre* transgenes capable of transient Cre expression (e.g., CreER) might substantially reduce this effect and improve the robustness of the model.

Although p53 activity in HSCs can suppress HCC, it remains unclear whether or not mutational disruption of this program is relevant during the natural HCC progression. In principle, the high rate of cell turnover in damaged livers could lead to the selection of *p53* mutant HSCs, though currently there is no indication that *p53* mutations are present in cells associated with the fibrotic lesions adjacent to liver tumors. However, in other contexts, *p53* mutations have been observed in stromal cells in both mice and humans (Hill et al., 2005; Kurose et al., 2002), suggesting that such a possibility cannot be excluded. Regardless, the fact that a non-cell-autonomous stromal program can suppress organ damage and epithelial cell transformation provides a new avenue for exploiting knowledge of the p53 network in controlling ''fibrosis-cirrhosis-carcinoma'' progression.

Our data imply that p53 acts non-cell autonomously to promote an antitumorigenic tissue microenvironment. Engagement of p53 in activated murine HSCs triggers an antiproliferative program that manifests the features of senescence observed in other cell types; these features include global changes in the expression of cell-cycle regulators, SASP, and production of immune modulators that were previously linked to fibrosis resolution (Krizhanovsky et al., 2008). Of note, whereas others reported a general suppression of the secretory phenotype by p53 in senescent fibroblasts (Coppé et al., 2008), we observed decisively qualitative effects in HSCs, which included a significant switch in the cytokines produced by senescent versus proliferating cells.

The most prominent effects observed involved factors that influence macrophage biology. Indeed, the senescent state triggered by p53 caused a significant increase in the secretion of factors known to promote M1 polarization, which is characterized by *Il1β* expression and an increased propensity for cell killing and phagocytosis (Biswas and Mantovani, 2010). By marked contrast, p53 suppressed the secretion of factors associated with M2 polarization. Accordingly, CM from p53-expressing HSCs promoted M1 polarization of macrophages, which then acquired the ability to target senescent HSCs. Conversely, CM from proliferating HSCs with suppressed p53 activity stimulated M2 polarization of macrophages, which were unable to target HSCs but could stimulate the proliferation of premalignant hepatoblasts.

The action of p53 in stimulating an antitumor microenvironment is likely to involve both direct and indirect mechanisms. On one hand, several immune-modulatory factors upregulated in HSCs undergoing senescence are direct p53 transcriptional targets. However, p53 also has a complex but well-established role in coordinating gene expression together with NF-κB, an immune modulating transcription factor. The impact of this intersection is context dependent, with some studies suggesting that NF-κB can antagonize p53 function, whereas others imply that it can complement certain p53 effects. During senescence, p53 and NF-κB cooperate in the execution of the program (Chien et al., 2011; Jing et al., 2011), and, as shown here, this interplay influences macrophage polarization and the subsequent targeting of senescent cells. Precisely how this occurs remains to be determined and likely involves a direct effect of p53 on the transcription of NF-κB-activating factors as well as unidentified indirect effects.

Beyond its effects on macrophages, p53 signaling likely influences the microenvironment in additional ways. For example, cells triggered to senesce by p53 can recruit NK cells and cytotoxic T lymphocytes into inflammatory sites enhancing immune

surveillance and can limit the production of new blood vessels through the induction of antiangiogenic molecules (Dameron et al., 1994; Kang et al., 2011; Krizhanovsky et al., 2008). In promoting these processes, p53 acts in a quantitative way to augment recruitment of immune cells or tumor inhibitory factors. By contrast, the effects of p53-driven SASP on macrophage polarization are unique in that they qualitatively alter macrophage function, an effect that can be observed in damaged livers in vivo.

Our studies support a model whereby normal p53 activity in HSCs acts to limit the extent of liver damage and to help maintain organ integrity through its impact on SASP. Among the many factors that contribute to this effect, macrophages have long been considered to be crucial for the formation of the fibrotic scar and, paradoxically, for the resolution of fibrosis (Duffield et al., 2005; Ramachandran et al., 2012). An intriguing possibility is that the differential effect of proliferating and senescent HSCs on macrophage polarization underlies their opposing role in liver damage responses. In this scenario, liver damage activates HSC proliferation, which promotes the recruitment and M2 polarization of macrophages that stimulate fibrosis as part of the tissue-remodeling and proangiogenic response that maintains organ integrity. Subsequently, p53 activation and senescence in HSCs could favor M1 polarization of macrophages that counteracts these effects by promoting an antifibrogenic environment and elimination of accumulated HSCs. In the presence of chronic liver damage, proliferating HSCs that fail to activate p53 would continue to accumulate, biasing macrophage populations in the liver to the tumorigenic M2 subtype that can also enhance the proliferation of premalignant cells. Consistent with this view, M2 macrophages accumulate in patients with chronic liver disease (Zimmermann et al., 2011), whereas the accumulation of M1 macrophages has been linked to reduced fibrosis (Hesse et al., 2000).

We propose that the non-cell-autonomous action of p53 in HCC is an inadvertent consequence of its action in this natural wound healing response. Thus, the same factors that influence wound resolution create a microenvironment that resists epithelial cell transformation through a variety of mechanisms including, as shown here, an increase in production of antitumor modulators and cell types. However, upon chronic damage, an inherently protumorigenic milieu created by M2 macrophages and by other factors affected by proliferating HSCs predominates and creates an environment prone to epithelial cell transformation. Although further studies are needed, the fact that p53 can communicate a tumor-suppressive program through soluble components that modify the tissue microenvironment offers insights into this well-characterized tumor-suppressor network and provides optimism that these effects might eventually be phenocopied therapeutically for improving liver function and reducing liver cancer incidence.

EXPERIMENTAL PROCEDURES

Animals and Housing

Animal work was conducted in accordance with protocols approved by the Institutional Animal Care and Use Committees at CSHL and MSKCC. Mice were maintained under specific pathogen-free conditions, and food and water were provided ad libitum. Animal treatment details are in Extended Experimental Procedures.

Histological Analysis

Paraffin-embedded tissue sections were stained with H&E for routine examination, Sirius red for visualization of fibrotic deposition, and Gordon and Sweet's for Reticulin. At least three whole sections from each animal were scanned with Laser Scanner Cytometry (CompuCyte; Aperio) for fibrosis analysis. The images were quantified using NIH ImageJ software (http://rsb.info.nih.gov/ij/). The amount of fibrotic tissue was calculated relative to the total analyzed liver area. Detection of transgenic-β-gal activity was performed as previously described at pH = 7.4 (Krizhanovsky et al., 2008).

Tissue Culture

HSCs were grown in DMEM supplemented with 10% FBS, 1% glutamine, 100 U/ml penicillin, 100 μg/ml streptomycin, and 1 μg/ml doxycycline (Dox). Senescence was induced by withdrawing Dox, replicative exhaustion, or by adding etoposide (100 μM, Sigma). Detection of senescence-associated β-gal activity was performed as previously described at pH = 5.5 (Krizhanovsky et al., 2008). Cell isolation and cytotoxicity experiments are described in Extended Experimental Procedures.

Quantitative RT-PCR and Expression Array Analysis

Murine HSCs, primary BMDMs, or sorted macrophages were freshly homogenized in Trizol (GIBCO). RNA isolation, cDNA synthesis, and quantitative RT-PCRs were performed as previously described (Xue et al., 2007). Microarray experiments were performed on Mouse Genome 430A 2.0 Arrays (Affymetrix) at MSKCC Genomics Core. GSEA analysis was performed using GSEA v2.07 software with 1,000 phenotype permutations. For GO term analysis, DAVID Bioinformatics Resources 6.7 was utilized at http://david.abcc.ncifcrf.gov/home.jsp. Gene sets used in this study, technical details, and the list of Taqman probes are included in Table S1 and Extended Experimental Procedures.

Immunoblotting

Liver tissues were lysed in Laemmli buffer using a tissue homogenizer. Cellular lysates from HSCs or macrophages were also prepared by lysing with Laemmli buffer. Equal amounts of protein were separated on 12% SDS-polyacrylamide gels and transferred to PVDF membranes. The abundance of β-actin was monitored to ensure equal loading. Images were analyzed using the NIH Image J software. Immunofluorescence staining was performed as previously described (Chien et al., 2011). Alexa Fluor conjugates (Molecular Probes) were used as the secondary antibodies, and DNA was visualized with 49-6-diamidino-2-phenylindole (DAPI; Vector Laboratories). The details of fluorescence quantification and the list of antibodies can be found in Extended Experimental Procedures.

Sorting of Macrophages

Livers from CCl_4-treated animals were digested with dispase (0.2%, GIBCO) in HBSS during 30 min at 37°C and then filtered through a 100 μm mesh filter. Red blood cells were eliminated by washing with 1× RBC Lysis Buffer (eBioscience). Samples were then washed with FACS buffer (1% BSA in PBS), followed by Fc block for 15 min at 4°C and antibody labeling for 15 min at 4°C. Antibodies used for cell type identification were CD45-APC (1:500; BD Biosciences PharMingen), Gr1-FITC (1:500; BD Biosciences PharMingen), and Cd11b-PE (1:500; BD Biosciences PharMingen). FACS buffer with DAPI (Invitrogen) was then added to each sample, followed by acquisition and sorting on an Aria1 sorter (BD).

Statistics

Statistical significance was calculated by two-tailed Student's t test. Log rank test was used to determine overall and pairwise significance for survival curves. Interaction between CM and BMDM effects was calculated with two-way ANOVA. Prism 5 Software was used for the generation of the survival graphs and statistical analyses. Significance values are $*p < 0.05$, $**p < 0.01$, and $***p < 0.001$. Ns stands for nonsignificant ($p > 0.05$).

ACCESSION NUMBERS

All raw microarray data files are available in the GEO database (GSE39469).

SUPPLEMENTAL INFORMATION

Supplemental Information includes Extended Experimental Procedures, seven figures, one table, and four movies and can be found with this article online at http://dx.doi.org/10.1016/j.cell.2013.03.020.

ACKNOWLEDGMENTS

We gratefully thank Jacqueline Cappellani and Sha Tian for excellent technical assistance; Prem Premsrirut for generating the TG-p53.1224 mouse strain; Orit Pappo for advice in pathological analyses; Vadim Pinskiy and Anna Chuprin for scanning the slides; Carolyn Zawislak for help with NK cell isolation; Anna Sabarovsky for assistance with ultrasound imaging; and Eusebio Manchado, Geulah Livshits, Shane Mayack, and Charles Sherr for constructive criticisms and careful editing of the manuscript. We also thank members of the Lowe laboratory for stimulating discussions. We thank CSHL and MSKCC animal facilities, CSHL histology facility, MSKCC Molecular Cytology Core, and MSKCC Genomics Core. A.L. is funded by EMBO-Long-Term Fellowship; J.A.J. and L.A. are funded by NCI U54 CA148967; D.F.T. is funded by the German Research Foundation (DFG); and V.K. is an incumbent of The Karl and Frances Korn Career Development Chair at Weizmann Institute of Science and is supported by Israel Science Foundation. S.W.L. is the Geoffrey Beene chair for Cancer Biology and is a Howard Hughes Medical Institute investigator. This work was supported by AG16379 grant from the NIA.

Received: August 6, 2012
Revised: January 16, 2013
Accepted: March 14, 2013
Published: April 4, 2013

REFERENCES

Acosta, J.C., O'Loghlen, A., Banito, A., Guijarro, M.V., Augert, A., Raguz, S., Fumagalli, M., Da Costa, M., Brown, C., Popov, N., et al. (2008). Chemokine signaling via the CXCR2 receptor reinforces senescence. Cell *133*, 1006–1018.

Bataller, R., and Brenner, D.A. (2005). Liver fibrosis. J. Clin. Invest. *115*, 209–218.

Biswas, S.K., and Mantovani, A. (2010). Macrophage plasticity and interaction with lymphocyte subsets: cancer as a paradigm. Nat. Immunol. *11*, 889–896.

Campisi, J., and d'Adda di Fagagna, F. (2007). Cellular senescence: when bad things happen to good cells. Nat. Rev. Mol. Cell Biol. *8*, 729–740.

Chien, Y., Scuoppo, C., Wang, X., Fang, X., Balgley, B., Bolden, J.E., Premsrirut, P., Luo, W., Chicas, A., Lee, C.S., et al. (2011). Control of the senescence-associated secretory phenotype by NF-κB promotes senescence and enhances chemosensitivity. Genes Dev. *25*, 2125–2136.

Collado, M., and Serrano, M. (2010). Senescence in tumours: evidence from mice and humans. Nat. Rev. Cancer *10*, 51–57.

Coppé, J.P., Patil, C.K., Rodier, F., Sun, Y., Muñoz, D.P., Goldstein, J., Nelson, P.S., Desprez, P.Y., and Campisi, J. (2008). Senescence-associated secretory phenotypes reveal cell-nonautonomous functions of oncogenic RAS and the p53 tumor suppressor. PLoS Biol. *6*, 2853–2868.

Crescenzi, E., Pacifico, F., Lavorgna, A., De Palma, R., D'Aiuto, E., Palumbo, G., Formisano, S., and Leonardi, A. (2011). NF-κB-dependent cytokine secretion controls Fas expression on chemotherapy-induced premature senescent tumor cells. Oncogene *30*, 2707–2717.

Dameron, K.M., Volpert, O.V., Tainsky, M.A., and Bouck, N. (1994). Control of angiogenesis in fibroblasts by p53 regulation of thrombospondin-1. Science *265*, 1582–1584.

Duffield, J.S., Forbes, S.J., Constandinou, C.M., Clay, S., Partolina, M., Vuthoori, S., Wu, S., Lang, R., and Iredale, J.P. (2005). Selective depletion of macrophages reveals distinct, opposing roles during liver injury and repair. J. Clin. Invest. *115*, 56–65.

Forni, P.E., Scuoppo, C., Imayoshi, I., Taulli, R., Dastrù, W., Sala, V., Betz, U.A., Muzzi, P., Martinuzzi, D., Vercelli, A.E., et al. (2006). High levels of Cre expression in neuronal progenitors cause defects in brain development leading to microencephaly and hydrocephaly. J. Neurosci. *26*, 9593–9602.

Fridman, A.L., and Tainsky, M.A. (2008). Critical pathways in cellular senescence and immortalization revealed by gene expression profiling. Oncogene *27*, 5975–5987.

Hesse, M., Cheever, A.W., Jankovic, D., and Wynn, T.A. (2000). NOS-2 mediates the protective anti-inflammatory and antifibrotic effects of the Th1-inducing adjuvant, IL-12, in a Th2 model of granulomatous disease. Am. J. Pathol. *157*, 945–955.

Hill, R., Song, Y., Cardiff, R.D., and Van Dyke, T. (2005). Selective evolution of stromal mesenchyme with p53 loss in response to epithelial tumorigenesis. Cell *123*, 1001–1011.

Jing, H., Kase, J., Dörr, J.R., Milanovic, M., Lenze, D., Grau, M., Beuster, G., Ji, S., Reimann, M., Lenz, P., et al. (2011). Opposing roles of NF-κB in anti-cancer treatment outcome unveiled by cross-species investigations. Genes Dev. *25*, 2137–2146.

Kang, T.W., Yevsa, T., Woller, N., Hoenicke, L., Wuestefeld, T., Dauch, D., Hohmeyer, A., Gereke, M., Rudalska, R., Potapova, A., et al. (2011). Senescence surveillance of pre-malignant hepatocytes limits liver cancer development. Nature *479*, 547–551.

Kiaris, H., Chatzistamou, I., Trimis, G., Frangou-Plemmenou, M., Pafiti-Kondi, A., and Kalofoutis, A. (2005). Evidence for nonautonomous effect of p53 tumor suppressor in carcinogenesis. Cancer Res. *65*, 1627–1630.

Kong, X., Feng, D., Wang, H., Hong, F., Bertola, A., Wang, F.S., and Gao, B. (2012). Interleukin-22 induces hepatic stellate cell senescence and restricts liver fibrosis in mice. Hepatology *56*, 1150–1159.

Krtolica, A., Parrinello, S., Lockett, S., Desprez, P., and Campisi, J. (2001). Senescent fibroblasts promote epithelial cell growth and tumorigenesis: A link between cancer and aging. Proc. Natl. Acad. Sci. USA *98*, 12072–12077.

Krizhanovsky, V., Yon, M., Dickins, R.A., Hearn, S., Simon, J., Miething, C., Yee, H., Zender, L., and Lowe, S.W. (2008). Senescence of activated stellate cells limits liver fibrosis. Cell *134*, 657–667.

Kuilman, T., Michaloglou, C., Vredeveld, L.C., Douma, S., van Doorn, R., Desmet, C.J., Aarden, L.A., Mooi, W.J., and Peeper, D.S. (2008). Oncogene-induced senescence relayed by an interleukin-dependent inflammatory network. Cell *133*, 1019–1031.

Kurose, K., Gilley, K., Matsumoto, S., Watson, P.H., Zhou, X.P., and Eng, C. (2002). Frequent somatic mutations in PTEN and TP53 are mutually exclusive in the stroma of breast carcinomas. Nat. Genet. *32*, 355–357.

Lee, J.S., Chu, I.S., Mikaelyan, A., Calvisi, D.F., Heo, J., Reddy, J.K., and Thorgeirsson, S.S. (2004). Application of comparative functional genomics to identify best-fit mouse models to study human cancer. Nat. Genet. *36*, 1306–1311.

Li, T., Kon, N., Jiang, L., Tan, M., Ludwig, T., Zhao, Y., Baer, R., and Gu, W. (2012). Tumor suppression in the absence of p53-mediated cell-cycle arrest, apoptosis, and senescence. Cell *149*, 1269–1283.

Marino, S., Vooijs, M., van Der Gulden, H., Jonkers, J., and Berns, A. (2000). Induction of medulloblastomas in p53-null mutant mice by somatic inactivation of Rb in the external granular layer cells of the cerebellum. Genes Dev. *14*, 994–1004.

Movahedi, K., Laoui, D., Gysemans, C., Baeten, M., Stangé, G., Van den Bossche, J., Mack, M., Pipeleers, D., In't Veld, P., De Baetselier, P., and Van Ginderachter, J.A. (2010). Different tumor microenvironments contain functionally distinct subsets of macrophages derived from Ly6C(high) monocytes. Cancer Res. *70*, 5728–5739.

Naugler, W.E., Sakurai, T., Kim, S., Maeda, S., Kim, K., Elsharkawy, A.M., and Karin, M. (2007). Gender disparity in liver cancer due to sex differences in MyD88-dependent IL-6 production. Science *317*, 121–124.

Oakley, F., Mann, J., Nailard, S., Smart, D.E., Mungalsingh, N., Constandinou, C., Ali, S., Wilson, S.J., Millward-Sadler, H., Iredale, J.P., and Mann, D.A. (2005). Nuclear factor-kappaB1 (p50) limits the inflammatory and fibrogenic responses to chronic injury. Am. J. Pathol. *166*, 695–708.

Ohtsuka, T., Ryu, H., Minamishima, Y.A., Macip, S., Sagara, J., Nakayama, K.I., Aaronson, S.A., and Lee, S.W. (2004). ASC is a Bax adaptor and regulates the p53-Bax mitochondrial apoptosis pathway. Nat. Cell Biol. *6*, 121–128.

Premsrirut, P.K., Dow, L.E., Kim, S.Y., Camiolo, M., Malone, C.D., Miething, C., Scuoppo, C., Zuber, J., Dickins, R.A., Kogan, S.C., et al. (2011). A rapid and scalable system for studying gene function in mice using conditional RNA interference. Cell *145*, 145–158.

Qian, B.Z., and Pollard, J.W. (2010). Macrophage diversity enhances tumor progression and metastasis. Cell *141*, 39–51.

Ramachandran, P., Pellicoro, A., Vernon, M.A., Boulter, L., Aucott, R.L., Ali, A., Hartland, S.N., Snowdon, V.K., Cappon, A., Gordon-Walker, T.T., et al. (2012). Differential Ly-6C expression identifies the recruited macrophage phenotype, which orchestrates the regression of murine liver fibrosis. Proc. Natl. Acad. Sci. USA *109*, E3186–E3195.

Reimann, M., Lee, S., Loddenkemper, C., Dörr, J.R., Tabor, V., Aichele, P., Stein, H., Dörken, B., Jenuwein, T., and Schmitt, C.A. (2010). Tumor stroma-derived TGF-beta limits myc-driven lymphomagenesis via Suv39h1-dependent senescence. Cancer Cell *17*, 262–272.

Ryan, K.M., Ernst, M.K., Rice, N.R., and Vousden, K.H. (2000). Role of NF-kappaB in p53-mediated programmed cell death. Nature *404*, 892–897.

Tanikawa, C., Furukawa, Y., Yoshida, N., Arakawa, H., Nakamura, Y., and Matsuda, K. (2009). XEDAR as a putative colorectal tumor suppressor that mediates p53-regulated anoikis pathway. Oncogene *28*, 3081–3092.

Trimboli, A.J., Cantemir-Stone, C.Z., Li, F., Wallace, J.A., Merchant, A., Creasap, N., Thompson, J.C., Caserta, E., Wang, H., Chong, J.L., et al. (2009). Pten in stromal fibroblasts suppresses mammary epithelial tumours. Nature *461*, 1084–1091.

Vousden, K.H., and Prives, C. (2009). Blinded by the light: the growing complexity of p53. Cell *137*, 413–431.

Xue, W., Zender, L., Miething, C., Dickins, R.A., Hernando, E., Krizhanovsky, V., Cordon-Cardo, C., and Lowe, S.W. (2007). Senescence and tumour clearance is triggered by p53 restoration in murine liver carcinomas. Nature *445*, 656–660.

Zender, L., Xue, W., Zuber, J., Semighini, C.P., Krasnitz, A., Ma, B., Zender, P., Kubicka, S., Luk, J.M., Schirmacher, P., et al. (2008). An oncogenomics-based in vivo RNAi screen identifies tumor suppressors in liver cancer. Cell *135*, 852–864.

Zhang, D.Y., and Friedman, S.L. (2012). Fibrosis-dependent mechanisms of hepatocarcinogenesis. Hepatology *56*, 769–775.

Zimmermann, H.W., Seidler, S., Gassler, N., Nattermann, J., Luedde, T., Trautwein, C., and Tacke, F. (2011). Interleukin-8 is activated in patients with chronic liver diseases and associated with hepatic macrophage accumulation in human liver fibrosis. PLoS ONE *6*, e21381.